JOURNAL OF VIROLOGY, Aug. 2008, p. 8071–8084 Vol. 82, No. 16
0022-538X/08/$08.00+0 doi:10.1128/JVI.00407-08

Coronavirus Nonstructural Protein 16 Is a Cap-0 Binding Enzyme Possessing (Nucleoside-2′*O*)-Methyltransferase Activity▽

Etienne Decroly,[1]*† Isabelle Imbert,[1]† Bruno Coutard,[1] Mickaël Bouvet,[1] Barbara Selisko,[1] Karine Alvarez,[1] Alexander E. Gorbalenya,[2] Eric J. Snijder,[2] and Bruno Canard[1]*

Architecture et Fonction des Macromolécules Biologiques, CNRS, and Universités d'Aix-Marseille I et II, UMR 6098, ESIL Case 925, 13288 Marseille, France,[1] and Molecular Virology Laboratory, Department of Medical Microbiology, Center of Infectious Diseases, Leiden University Medical Center, LUMC P4-26, P.O. Box 9600, 2300 RC Leiden, The Netherlands[2]

Received 25 February 2008/Accepted 8 April 2008

The coronavirus family of positive-strand RNA viruses includes important pathogens of livestock, companion animals, and humans, including the severe acute respiratory syndrome coronavirus that was responsible for a worldwide outbreak in 2003. The unusually complex coronavirus replicase/transcriptase is comprised of 15 or 16 virus-specific subunits that are autoproteolytically derived from two large polyproteins. In line with bioinformatics predictions, we now show that feline coronavirus (FCoV) nonstructural protein 16 (nsp16) possesses an *S*-adenosyl-L-methionine (AdoMet)-dependent RNA (nucleoside-2′*O*)-methyltransferase (2′*O*-MTase) activity that is capable of cap-1 formation. Purified recombinant FCoV nsp16 selectively binds to short capped RNAs. Remarkably, an N7-methyl guanosine cap (^{7Me}GpppAC$_{3-6}$) is a prerequisite for binding. High-performance liquid chromatography analysis demonstrated that nsp16 mediates methyl transfer from AdoMet to the 2′*O* position of the first transcribed nucleotide, thus converting ^{7Me}GpppAC$_{3-6}$ into ^{7Me}GpppA$_{2'OMe}$C$_{3-6}$. The characterization of 11 nsp16 mutants supported the previous identification of residues K45, D129, K169, and E202 as the putative K-D-K-E catalytic tetrad of the enzyme. Furthermore, residues Y29 and F173 of FCoV nsp16, which may be the functional counterparts of aromatic residues involved in substrate recognition by the vaccinia virus MTase VP39, were found to be essential for both substrate binding and 2′*O*-MTase activity. Finally, the weak inhibition profile of different AdoMet analogues indicates that nsp16 has evolved an atypical AdoMet binding site. Our results suggest that coronavirus mRNA carries a cap-1, onto which 2′*O* methylation follows an order of events in which 2′*O*-methyl transfer must be preceded by guanine N7 methylation, with the latter step being performed by a yet-unknown N7-specific MTase.

The family *Coronaviridae*, comprising the genera *Coronavirus* and *Torovirus*, belongs to the order *Nidovirales*, a lineage of positive-strand RNA viruses that also includes the *Arteriviridae* and *Roniviridae* families (for a review, see reference 28). Coronaviruses (CoV) are frequently associated with respiratory and enteric diseases in humans, livestock, and companion animals. In recent years, they received worldwide attention following both the 2003 outbreak caused by the emerging severe acute respiratory syndrome CoV (SARS-CoV) (17, 43, 57) and the subsequent identification of several other novel family members, including two additional human pathogens (63). On the basis of antigenic and genetic analyses, CoV have been divided into three groups (29), with group 3 representing avian CoV and group 2 including viruses like murine hepatitis virus (MHV), the human CoV (HCoV) OC43 and HKU1, and SARS-CoV. CoV group 1 includes, among others, the HCoV 229E and NL63, the porcine transmissible gastroenteritis virus, and canine and feline CoV (FCoV). Infection with FCoV is very common in cats and kittens. Although FCoV infection usually is transient, resulting in a mild gastrointestinal disease, the virus may persist in a significant percentage of cases (1). A small proportion of FCoV-infected cats develop a lethal, immune-mediated disease that is known as feline infectious peritonitis (FIP). The basis for virulence has remained controversial, with one suggestion being that FIP virus (FIPV) arises when a persistently infecting, enteric FCoV acquires mutations that increase its virulence (81).

As for other nidoviruses, the large genome of CoV (27 to 32 kb) is polycistronic, with about two-thirds being occupied by two large replicase open reading frames (ORF1a and ORF1b) that encode the viral nonstructural proteins (nsps). The genes downstream of the replicase ORFs encode structural and virus-specific accessory proteins (for a review, see reference 28). Genome expression starts with the translation of ORF1a and ORF1b, presumably by a cap-dependent mechanism (44, 80), with the expression of ORF1b involving a −1 ribosomal frameshift (9). The two resulting replicase polyproteins, pp1a and pp1ab, are processed by two or three viral proteases to generate 16 end products, termed nsp1 to nsp16 (28, 76, 87). These cleavage products assemble into a large, membrane-anchored multienzyme complex, termed the replication-transcription complex, that mediates all functions required for genome replication and subgenomic mRNA synthesis (38, 78, 79). The replication-transcription complex includes enzyme functions commonly found in positive-strand RNA viruses, like an RNA-dependent RNA polymerase (nsp12 [13]), proteases (nsp3 and

* Corresponding author. Mailing address: Architecture et Fonction des Macromolécules Biologiques, CNRS and Universités d'Aix-Marseille I et II, UMR 6098, ESIL Case 925, 13288 Marseille, France. Phone: 33 491 82 86 44. Fax: 33 491 82 86 46. E-mail for E. Decroly: etienne.decroly@afmb.univ-mrs.fr. E-mail for B. Canard: bruno.canard@afmb.univ-mrs.fr.
† These authors contributed equally to this work.
▽ Published ahead of print on 16 April 2008.

nsp5 [4, 49]), and a helicase/RNA triphosphatase (nsp13 [40, 73]). Additionally, the CoV genome encodes a set of RNA-processing activities that either are unique to certain nidovirus subgroups or are found in only a few other groups of RNA viruses (76). These functions include an ADP-ribose phosphatase (X or *macro* domain in nsp3 [62]), a recently discovered putative RNA primase (nsp8 [37]), an exoribonuclease (nsp14 [54]), and a nidovirus uridylate-specific endoribonuclease (NendoU in nsp15 [39]).

This group of enzymes also includes the functionally uncharacterized nsp16, which was predicted to be an *S*-adenosyl-L-methionine (AdoMet)-dependent RNA (nucleoside-2′*O*)-methyltransferase (2′*O*-MTase) (53, 76, 82). It contains a highly conserved catalytic tetrad (K-D-K-E) that is a hallmark of RNA 2′*O*-MTases (12, 19, 22, 23). A three-dimensional model of the MTase core of SARS-CoV nsp16 was generated by a structure prediction server (3D jury meta predictor) using the 2′*O*-MTase domain of the reovirus protein λ2 as a template (82). Based on the role of its homologues in other RNA viruses, nsp16 was postulated to be involved in mRNA capping (76, 82). Alternatively, but not mutually exclusively, it was proposed that nsp16 2′*O* methylates selected nucleosides in virus and/or cellular RNAs as part of a pathway that could involve other unique CoV RNA-processing enzymes (76). Somewhat compatible with this hypothesis, RNA cleavage by the nsp15 NendoU was found to be inhibited by 2′*O*-methylation (39). Whereas the exact role of nsp16 during CoV replication still is unknown, its functional importance was supported by mutagenesis experiments using a SARS-CoV replicon system (3). The deletion of the nsp16 coding sequence blocked RNA synthesis, whereas a single mutation in the catalytic tetrad reduced replicon-driven mRNA synthesis to about 10% of the level for the wild type (wt). Moreover, the phenotype of temperature-sensitive MHV mutants suggested that nsp16 has an essential role in either the synthesis or stability of viral RNA or in controlling a cellular function that is able to limit virus replication (70). Elucidating the specific biochemical properties of nsp16 clearly would help to assess its role and importance in the viral life cycle.

The RNA cap is a unique structure found at the 5′ end of eukaryotic cellular and many viral messenger RNAs. In eukaryotic cells, the cap structure protects mRNA from degradation by 5′ exoribonucleases and enhances the initiation of mRNA translation (24, 75). For nascent cellular transcripts, the addition of the cap-0 structure is a cotranscriptional event that occurs in the nucleus. Cap-0 formation generally requires three sequential enzymatic activities: (i) an RNA 5′-triphosphatase (RTPase) that removes the 5′ γ-phosphate group of the mRNA; (ii) a guanylyltransferase (GTase), or capping enzyme, that catalyzes the transfer of GMP to the remaining 5′-diphosphate end; and (iii) an AdoMet-dependent (guanine-N7)-MTase (N7-MTase) that methylates the cap at the N7 position. Whereas lower eukaryotes, including yeast, employ a cap-0 structure, higher eukaryotes convert cap-0 into cap-1 or cap-2 structures (46) by means of a nuclear AdoMet-dependent 2′*O*-MTase that methylates the ribose 2′*O* position of the first and second nucleotide of the mRNA, respectively.

Many viruses that replicate in the cytoplasm encode their own RNA capping machinery. Some of these viruses, such as the positive-sense single-stranded RNA (ssRNA) flaviviruses (20, 66) and DNA poxviruses (84), seem to have adopted the sequential four-step mechanism used in eukaryotic mRNA cap-1 formation. However, the molecular and genetic organization of the enzymatic activities involved in RNA capping varies between virus groups. For example, in the poxvirus vaccinia virus (VV), cap-0 formation is catalyzed by a single 95-kDa protein encoded by viral gene D1 (21, 31, 74, 84). The subsequent methylation of capped RNA at the 2′*O* position requires VP39, a bifunctional protein that also directs 3′ polyadenylation (71). In contrast, in flaviviruses, an RTPase activity is found in the C-terminal domain of the multifunctional helicase protein NS3 (7, 8), whereas the two MTase activities (the N7- and 2′*O*-MTases) reside in the N-terminal domain of the RNA-dependent RNA polymerase subunit NS5 (19, 66). There also are RNA viruses with capping mechanisms that deviate dramatically from the canonical pathway. Alphaviruses may use an alternative pathway for mRNA capping, in which the GTP molecule is methylated before being transferred to the 5′-diphosphate end of viral RNAs (2). Yet another unconventional mechanism is employed by the rhabdovirus vesicular stomatitis virus (VSV), which involves a unique polyribonucleotidyltransferase activity to transfer the monophosphate mRNA onto GDP derived from GTP (55).

CoV not only have a genomic mRNA but also produce an extensive nested set of subgenomic mRNAs, a property that emphasizes the importance of the presumed RNA capping process (for recent reviews, see references 56 and 69). On the basis of T1-oligonucleotide fingerprinting, Lai and Stohlman previously claimed that the 5′ end of MHV mRNAs carries a cap structure (44). Moreover, using a cap-specific monoclonal antibody and exoribonuclease protection assays, it was demonstrated that both genomic and subgenomic mRNAs of equine torovirus carry a 5′ cap (80). However, the cap structure and the enzymes involved in CoV RNA capping and their mechanisms of action have not yet been characterized. The multifunctional nsp13 helicase subunit possibly is involved, which was previously shown to carry an RNA 5′-triphosphatase activity in the case of both group 1 and group 2 CoV (HCoV-229E and SARS-CoV) (40, 41). As for several other groups of RNA viruses, the GTase involved has not yet been identified. In addition to the predicted nsp16-mediated 2′*O*-MTase activity (76, 82), it was suggested that the SUD (for *S*ARS-CoV *u*nique *d*omain) of SARS-CoV nsp3 exhibits N7-MTase activity (26). This prediction, which has not been verified experimentally, is weakened by the fact that this domain is conserved only in group 2b CoV (A. E. Gorbalenya, unpublished data). Thus, the identification of the N7-MTase as well as other CoV capping factors remains to be achieved.

In this paper, we provide the first experimental evidence for the AdoMet-dependent 2′*O*-MTase activity of a CoV nsp16. Using recombinant FCoV nsp16 and short capped and uncapped RNAs, we show that this enzyme has selective RNA binding properties and demonstrate that it is a cap-0 (^{7Me}GpppAC$_5$) binding protein. Using site-directed mutagenesis, we confirm the essential role of the conserved K-D-K-E catalytic tetrad for mRNA cap 2′*O*-MTase activity and identify aromatic residues in the nsp16 N terminus that may play a key role in cap-0 binding. Finally, the weak inhibition profile of AdoMet analogues that are known potent MTase inhibitors suggests the presence of a unique methyl donor binding site in

an otherwise conserved three-dimensional MTase domain organization.

MATERIALS AND METHODS

Cloning of the FCoV nsp16 gene. FCoV strain FIPV WSU-79/1146 (GenBank accession no. DQ010921) (18) was kindly provided by Stuart Siddell (University of Bristol, United Kingdom) and was used to infect Crandell-Reese feline kidney cells. Intracellular RNA was isolated from infected cells and was used for the reverse transcription-PCR amplification of the nsp16 coding sequence (genome residues 19307 to 20206). The PCR primers used (sense, 5′-GGGGACAAGTTTGTACAAAAAAGCAGGCTTCGAAGGAGATAGAACCATGAAACATCACCATCACCATCACAGTTTAGAAAATGTGGCTTATA-3′; and antisense, 5′-GGGGACCACTTTGTACAAGAAAGCTGGGTCTTATTGTAGTTTTGGGTAGAAGGTT-3′) specified an N-terminal, in-frame hexahistidine tag and recombination sequences for use in the Gateway cloning system (Invitrogen). Following cloning into entry vector pDONR201 and sequence verification, the nsp16 gene was transferred to *Escherichia coli* expression vector pDest14 (Invitrogen) to give pDest14/6His-nsp16. Nsp16 mutagenesis was performed using the QuickChange site-directed mutagenesis kit (Stratagene) according to the manufacturer's instructions, followed by sequence verification (Millegen, France).

Reagents. AdoMet and adenosine-homocysteine (AdoHcy) were purchased from New England Biolabs. AdoMet analogues were obtained from Sigma-Aldrich. They were dissolved in dimethylsulfoxide (DMSO) and stored as 10 mM stock solutions at −20°C. α-^{32}P-labeled cytosine 5′-triphosphate (3,000 Ci/mmol), uniformly labeled [^{3}H]GTP (5.20 Ci/mmol), and 5′ triphosphate were purchased from GE Healthcare.

Expression and purification of NS5MTase$_{DV}$, hMTase, and FCoV nsp16. Recombinant NS5MTase$_{DV}$, corresponding to residues 1 to 296 of dengue virus (DV) NS5, was expressed and purified as described previously (19). The Human N7-guanine MTase (hN7-MTase) cDNA was a kind gift from Aaron J. Shatkin (Center of Advanced Biotechnology and Medicine, Piscataway, NJ). It was produced and purified as described previously (58).

E. coli C41(DE3) (Avidis SA, France), transformed with the pLysS plasmid (Novagen), was transformed with pDest14/6His-nsp16 and grown in Terrific broth (TB) containing ampicillin and chloramphenicol. When the optical density at 600 nm reached 0.6, isopropyl-β-D-thiogalactopyranoside was added to a final concentration of 0.5 mM, and expression was allowed to proceed for 18 h at 17°C. The bacterial cell pellet was resuspended in lysis buffer (50 mM Tris-HCl, pH 8.0, 300 mM NaCl, 5% glycerol, antiprotease cocktail [complete; Roche]) supplemented with 10 mM imidazole, 100 μg/ml lysozyme, 0.25 μg/ml Dnase I, and 0.1% Triton X-100. After lysis by sonication and clarification, immobilized metal affinity chromatography was used for the first purification step (chelating Sepharose fast-flow resin; GE Healthcare). FCoV nsp16 was eluted with 250 mM of imidazole in lysis buffer. Fractions containing nsp16 then were filtered (0.45-μm filter), loaded onto a Hi Load 16/60 Superdex 200 gel filtration column (GE Healthcare), and eluted with 10 mM HEPES, pH 7.5, 300 mM NaCl, 2 mM dithiothreitol (DTT), 50 mM arginine, and 50 mM glutamate. The fractions containing nsp16 were concentrated to 2 mg/ml on Amicon ultra 15 centrifugal filter units (10 kDa; Millipore) and stored at −20°C in the same buffer supplemented with 50% glycerol. The identity of wt nsp16 and mutants was checked by matrix-assisted laser desorption ionization–time of flight mass spectrometry after trypsin digestion (with wt nsp16 showing 43.2% of sequence coverage), by dynamic light scattering, and by sodium dodecyl sulfate-polyacrylamide gel electrophoresis (SDS-PAGE). All mutants, except for the poorly expressed W175A, were purified by the two-step procedure described above for wt nsp16. Mutant proteins showed gel filtration elution profiles similar to those of the wt control and were recovered as dimers from the column. Comparable amounts of each mutant protein were analyzed by SDS-PAGE (see Fig. 7B). Their electrophoretic mobility patterns were identical, except for that of the D129A mutant, which showed slightly aberrant migration in the gel (a 1- to 2-kDa decrease in apparent molecular mass).

RNA synthesis and purification. Capped and noncapped RNAs (^{7Me}GpppAC$_5$, GpppAC$_5$, and pppAC$_5$) were synthesized in vitro using bacteriophage T7 DNA primase and were purified by high-performance liquid chromatography (HPLC) as described previously (58). ^{32}P-labeled pppAC$_n$, ^{7Me}GpppAC$_n$, or GpppAC$_n$ RNA was synthesized as described previously (20). Reactions were stopped by adding RNase-free DNase I (500 U/ml for 30 min at 37°C; GE Healthcare) and proteinase K (100 μg/ml for 16 h at 37°C; Invitrogen) to remove the DNA template and the primase present in the reaction mixture. Proteinase K was inactivated at 70°C for 5 min. After 15 min of centrifugation at 16,000 × *g* in order to remove insoluble material, RNAs were resuspended in 100 μl of 10 mM Tris-HCl, pH 7.5, 50 mM NaCl, 2.5% glycerol, 500 μg/ml bovine serum albumin (BSA) and stored at −20°C.

MTase activity assays. Reactions for MTase activity assays were performed in 40 mM Tris-HCl, pH 7.5, 5 mM DTT, 2 μM ^{7Me}GpppAC$_n$ or GpppAC$_n$, 5 μM AdoMet, and 0.03 mCi/ml [^{3}H]AdoMet (GE Healthcare). $MgCl_2$ was added at a concentration of 1 mM for the standard nsp16 MTase assay. The reducing agent DTT (1 mM) was found to stabilize nsp16 activity over time (data not shown). NS5MTase$_{DV}$, hN7-MTase, and FCoV nsp16 were added at concentrations of 500 nM, 200 nM, and 3 μM, respectively, and reaction mixtures were incubated at 30°C and stopped after 4 h by a 10-fold dilution of the reaction mixture in 100 μM ice-cold AdoHcy. Samples were kept on ice and then transferred to glass-fiber filtermats (DEAE filtermat; Wallac) by a Filtermat Harvester (Packard Instruments). Filtermats were washed twice with 0.01 M ammonium formate, pH 8.0, twice with water, and once with ethanol, dried, and transferred into sample bags. Betaplate Scint (Wallac) scintillation fluid was added, and the methylation of RNA substrates was measured in counts per minute (cpm) by using a Wallac 1450 MicroBeta TriLux liquid scintillation counter. For inhibition assays, we set up the reaction as described above with a short RNA substrate (^{7Me}GpppAC$_5$) in the presence of various concentrations of candidate inhibitors. Enzymes and RNA substrates were mixed with the inhibitor before the addition of AdoMet to start the reaction. The final concentration of DMSO in the reaction mixtures was below 5%, and control reaction mixtures without inhibitor contained corresponding DMSO concentrations. Reaction mixtures were incubated at 30°C for 4 h. The samples then were transferred to glass-fiber filtermats (DEAE filtermat; Wallac) and counted as described above. The IC_{50} (inhibitor concentration at 50% activity) value of GTP, ^{7Me}GTP, and AdoHcy were determined using Kaleidagraph. Data were adjusted to a logistic dose-response function, % activity = $100/(1 + [I]/IC_{50})^b$, where *b* corresponds to the slope factor that determines the slope of the curve and [I] corresponds to the inhibitor concentration (15).

For HPLC analysis, reactions were performed in the absence of [^{3}H]AdoMet, and samples were mixed with 200 μl of triethylammonium bicarbonate solution (TEAB) (0.05 M) before HPLC analysis on a Waters model 600 gradient HPLC system. The column assembly consisted of a precolumn (Delta-pak C_{18}; 100 Å, 5 μm, 3.9 × 20 mm) and a separation column (Nova-pak C_{18}; 4 μm, 3.9 × 150 mm). For the on-line cleaning procedure, both columns were installed in parallel on a 7000 Rheodyne two-valve system (Interchim). Eluent A was a 0.05 M solution of TEAB (pH 7.4), and eluent B was a 1:1 (vol/vol) mixture of acetonitrile (HPLC grade; Carlo Erba SDS, France) and TEAB (final concentration, 0.05 M; pH 7.4). Separations were run at a flow rate of 1 ml/min and started with a 5-min elution (100% eluent A) on the precolumn to remove proteic material. The gradient started after 5 min at 100% eluent A, with an increase to 10% eluent B after 25 min and to 30% eluent B after 45 min.

Analysis of the ^{7Me}GpppAC$_5$ product by enzymatic digestion and HPLC. A preparative-scale reaction (800 μl) was performed using the standard conditions, and the reaction was stopped after overnight incubation. HPLC purification was performed as described above, and peaks corresponding to the reaction products were collected. Lyophilization was repeated three times, and 3 nmol of the reaction products was digested in a 60-μl reaction volume containing 50 mM Tris-HCl, pH 8.5, 5 mM $MgCl_2$, 0.3 U of nucleotide pyrophosphatase type II from *Crotalus adamanteus* (0.03 U in a 60-μl reaction volume; the enzyme preparation contained phosphodiesterase I side activity; Sigma) and 60 U of calf intestinal phosphatase (New England Biolabs). The digestion was allowed to proceed for 25 min at 37°C and was stopped by being heated to 95°C for 5 min. The digestion products then were separated by HPLC as described previously (58).

MTase binding assays. Binding assays were performed for 2 h at 4°C in binding buffer (10 mM Tris-HCl, pH 7.5, 50 mM NaCl, 2.5% glycerol, and 500 μg/ml BSA) in a total volume of 150 μl, as described previously (20). For competition experiments, incubation mixtures contained increasing concentrations of $MgCl_2$, ^{7Me}GTP, GTP, GpppA, or ^{7Me}GpppA. NS5MTase$_{DV}$ and FCoV nsp16 bound to nickel-nitrilotriacetic acid (Ni-NTA) beads were produced as described above. For each experiment, we used 30 μl of NS5MTase$_{DV}$ beads (≈4 μg/μl) and 10 μl of ^{32}P-radiolabeled RNA. Accordingly, 1 nmol of RNA was incubated with beads containing approximately 4 nmol of protein. After three washes with binding buffer, the RNA bound to the beads was liberated using 10 μl of formamide–EDTA gel loading buffer and separated by polyacrylamide gel electrophoresis (14% acrylamide-bisacrylamide [19:1], 7 M urea) in TTE buffer (89 mM Tris-HCl, pH 8.0, 28 mM taurine, 0.5 mM EDTA). RNA bands (with the input corresponding to 1/10 or 1/20 of the RNA incubated with NS5MTase$_{DV}$ beads) were visualized using photostimulated plates (fluorescent image analyzer FLA3000; Fuji).

Three-dimensional model of the nsp16 MTase core. Different Web servers employing threading and homology modeling (CPHmodels, Fugue, Phyre,

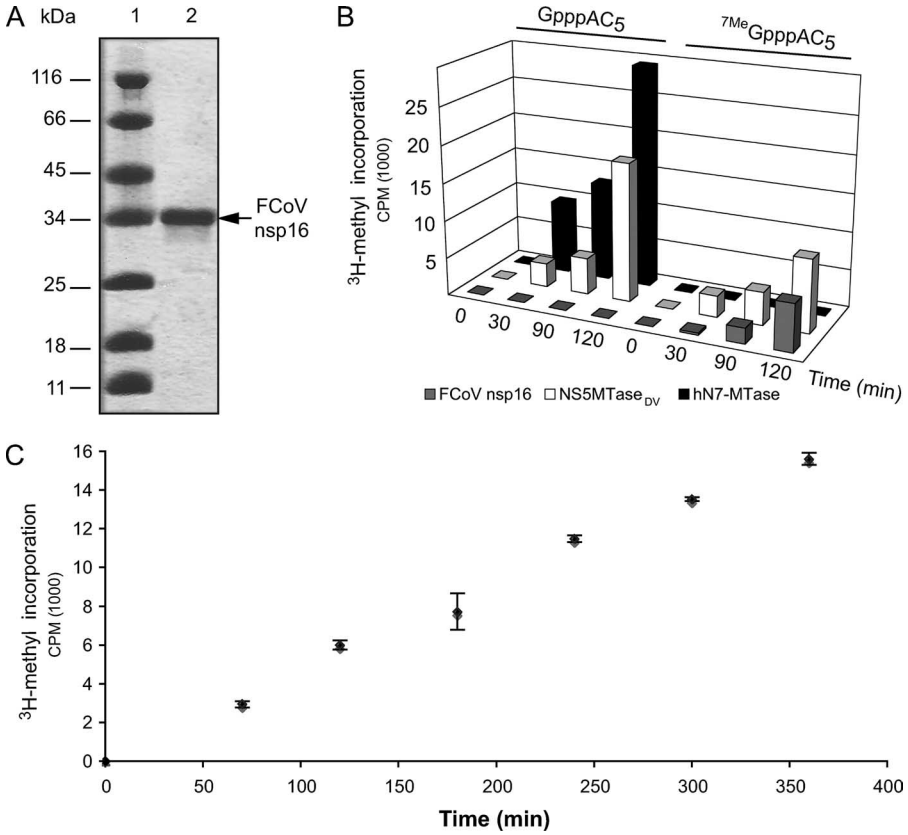

FIG. 1. Purification of FCoV nsp16 and AdoMet-dependent MTase assay. (A) A gel summarizing the purification of nsp16. After two chromatographic steps (see Materials and Methods), purified FCoV nsp16 protein was analyzed using 12% SDS–PAGE and the gel was stained using Coomassie blue. Lane 1 corresponds to the molecular mass marker and lane 2 to the final nsp16 protein preparation. (B) AdoMet-dependent MTase activity of hN7-MTase, $NS5MTase_{DV}$, and FCoV nsp16. Equal amounts of the different enzymes were incubated with $GpppAC_5$ and $^{7Me}GpppAC_5$ in the presence of [^{3}H]AdoMet. The methyl transfer to the RNA substrate was monitored during a 120-min time course and detected using a filter binding assay that measured the transferred amount of radioactivity in cpm. (C) Time course of the methylation reaction. FCoV nsp16 was incubated with $^{7Me}GpppAC_5$ in the presence of [^{3}H]AdoMet. The methyl transfer to the RNA substrate was monitored during 360 min and detected as described above.

ESyPred3D, HHpred, and LOOPP) were used to generate a model of FCoV nsp16. The closest template proposed by several servers was the rRNA 2′*O*-MTase FtsJ (Protein Data Bank identity no. [PDB ID] 1EIZ [11]), which served as the basis to generate a model using the HHpred server (http://toolkit.tuebingen.mpg.de/hhpred). K45 was added manually using TURBO (68).

RESULTS

Purified recombinant FCoV nsp16 protein is an AdoMet-dependent MTase. The CoV nsp16 previously was predicted to be a 2′*O*-MTase, therefore the enzyme was postulated to participate in cap-1 ($^{7Me}GpppN2'O_{Me}$) formation (76, 82). To experimentally verify the MTase activity, a cDNA sequence encoding FCoV nsp16 (300 amino acids; FCoV strain FIPV WSU-79/1146 [18]) was cloned and expressed in *E. coli* to produce a recombinant nsp16 that was $(His)_6$ tagged at its N terminus. The protein was purified by immobilized metal affinity chromatography, followed by size-exclusion chromatography in the presence of arginine and glutamate (each at 50 mM) in order to avoid protein precipitation (27). Upon gel filtration, the protein eluted as a single peak, corresponding to a size of about 65 kDa. In view of the calculated molecular mass of nsp16 and its migration as a single 35-kDa band during SDS-PAGE (Fig. 1A), this indicated that the purified protein probably was dimeric in solution. The identity of the recombinant protein was confirmed by matrix-assisted laser desorption ionization–time of flight mass spectrometry after trypsin digestion (data not shown).

To evaluate whether FCoV nsp16 exhibits MTase activity, we first incubated the purified protein with different short capped or uncapped RNA oligonucleotides ($^{7Me}GpppAC_5$, $GpppAC_5$, and $pppAC_5$) in the presence of the radiolabeled methyl donor [^{3}H]AdoMet. The first two nucleotides (AC) of the substrates were identical to the authentic 5′-terminal nucleotides of the FCoV genome (5′-ACUUUU. . .). As positive controls for MTase activity, we used hN7-MTase and $NS5MTase_{DV}$ (19, 58). Aliquots of the reaction mixtures were absorbed onto filters and washed, and the radioactivity that remained associated with the RNA substrate was measured to quantify its methylation.

No label was transferred to the uncapped $pppAC_5$ substrate, using either nsp16 or both control MTases (data not shown). As expected (58), $NS5MTase_{DV}$ shows MTase activity on both capped RNA substrates, whereas hN7-MTase methylated Gp $ppAC_5$ but not $^{7Me}GpppAC_5$ (Fig. 1B). In contrast, FCoV

nsp16 did not catalyze methyl transfer to either the guanine N7 or the 2′*O* position of the GpppAC$_5$ substrate. However, it was active on the capped ^{7Me}GpppAC$_5$ substrate and, thus, acted as an AdoMet-dependent mRNA cap MTase (Fig. 1B). From these observations, we conclude that FCoV nsp16 can transfer a methyl group to the 2′*O* position of the first and/or second nucleotide of an N7-methylated short RNA substrate. A time course experiment using FCoV nsp16 showed that, under our standard assay conditions, substrate accumulation was linear for at least 3 h (Fig. 1C) and then reached a plateau after overnight incubation (not shown).

We next characterized several parameters of the FCoV nsp16-mediated MTase activity. An analysis of the pH dependence of the enzyme produced a bell-shaped profile, with maximum activity observed at pH 7.5 (Fig. 2A). We also tested the dependence of the MTase on Mg^{2+} and Mn^{2+}, since these divalent cations previously were shown to promote *O*-methylation by some MTases (42). FCoV nsp16 MTase activity was modulated by the presence of either of the cations Mn^{2+} (not shown) or Mg^{2+} (Fig. 2B), with an optimum around a concentration of 1 mM. Finally, we tested the influence of the chain length of the capped substrate on nsp16 MTase activity. The protein was incubated with a variety of substrates, which differed in the number of cytidines at their 3′ ends (^{7Me}GpppAC$_n$, where n = 1 to 7), and [^{3}H]AdoMet for 4 h at 30°C. The nsp16-mediated methylation of RNA substrates again was measured using a filter binding assay. Figure 2C reveals a correlation between substrate length and MTase activity. The MTase activity increased with substrate length between 2 and 5 nucleotides (n = 1 to 4) and then reached a plateau. In order to exclude that the observed differences are due to the incomplete retention of small substrates on the filters used, the data were verified using HPLC analysis. To this end, nsp16 was incubated overnight with RNA and AdoMet, and the reaction products were separated by reverse-phase HPLC as described previously (58). The results were similar to those shown in Fig. 2C (data not shown). We conclude that, under the experimental conditions employed here, FCoV nsp16 exhibits the highest MTase activity at pH 7.5, in the presence of 1 mM Mg^{2+}, on capped RNA substrates of the ^{7Me}GpppAC$_n$ type, where n equals at least four.

FCoV nsp16 targets the 2′*O* position of the first transcribed nucleotide to produce a cap-1 structure. In order to identify the position(s) at which FCoV nsp16 methylates the ^{7Me}GpppAC$_5$ RNA substrate, we analyzed the reaction products by reverse-phase HPLC as described previously (58). As a control, we included NS5MTase$_{DV}$, which has been shown by mass spectrometry to methylate this substrate at the 2′*O* position of the first nucleotide (adenosine) and not onto downstream nucleotides (58). The retention time of the ^{7Me}GpppAC$_5$ substrate was 29.7 to 29.8 min (Fig. 3A). Two additional peaks appeared when the reaction products of FCoV nsp16 were analyzed: one was clearly ahead of the AdoHcy reaction product, probably being a degradation product of the latter, and the other had a retention time of 33.9 min (Fig. 3C). These two peaks, but not the one corresponding to the substrate, also were observed among the products generated by NS5MTase$_{DV}$, indicating that this enzyme methylated its substrate completely to yield ^{7Me}GpppA$_{2'OMe}$C$_5$ (58), which eluted at 33.9 min (Fig. 3B). These results indicated that both enzymes catalyzed strictly the same reaction on this capped RNA, albeit with different efficiencies.

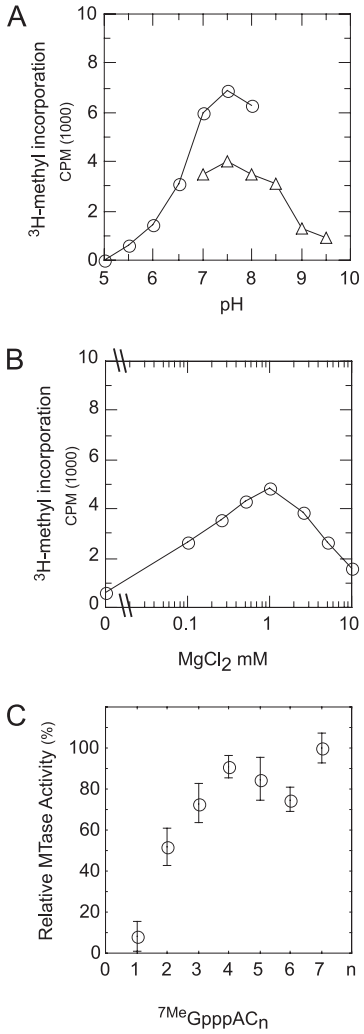

FIG. 2. Biochemical characterization of FCoV nsp16 AdoMet-dependent MTase activity. The FCoV nsp16 MTase activity was measured during a 120-min time course experiment by counting the amount of [^{3}H]methyl transferred onto the RNA substrate (^{7Me}GpppAC$_5$). (A) Enzyme activity in reactions in Tris buffer (pH 7 to 9; triangles) or Bis-Tris buffer (pH 5 to 8; circles). (B) FCoV nsp16 MTase activity in Tris-HCl buffer (pH 7.5) in the presence of increasing $MgCl_2$ concentrations. (C) FCoV nsp16 MTase activity after a 4-h incubation period using RNA substrates of increasing length (^{7Me}GpppAC$_{1-7}$). The cpm were normalized (100% corresponds to ^{7Me}GpppAC$_7$), and standard deviations were calculated from four independent experiments.

The study of the cap structure was further refined as follows. We collected the 33.9-min peak material, digested it enzymatically to release the corresponding nucleosides, and analyzed the resulting mixture using HPLC (Fig. 3D, lower chromatogram). The comparison to standard nucleosides (upper chromatogram) indicated that all adenosines present in the reaction product were methylated at the 2′*O* position. Two additional peaks (3.7 and 7.4 min) also were observed, with the major one (3.7 min) corresponding to unmethylated C and the minor one (7.4 min) remaining ambiguous, corresponding to

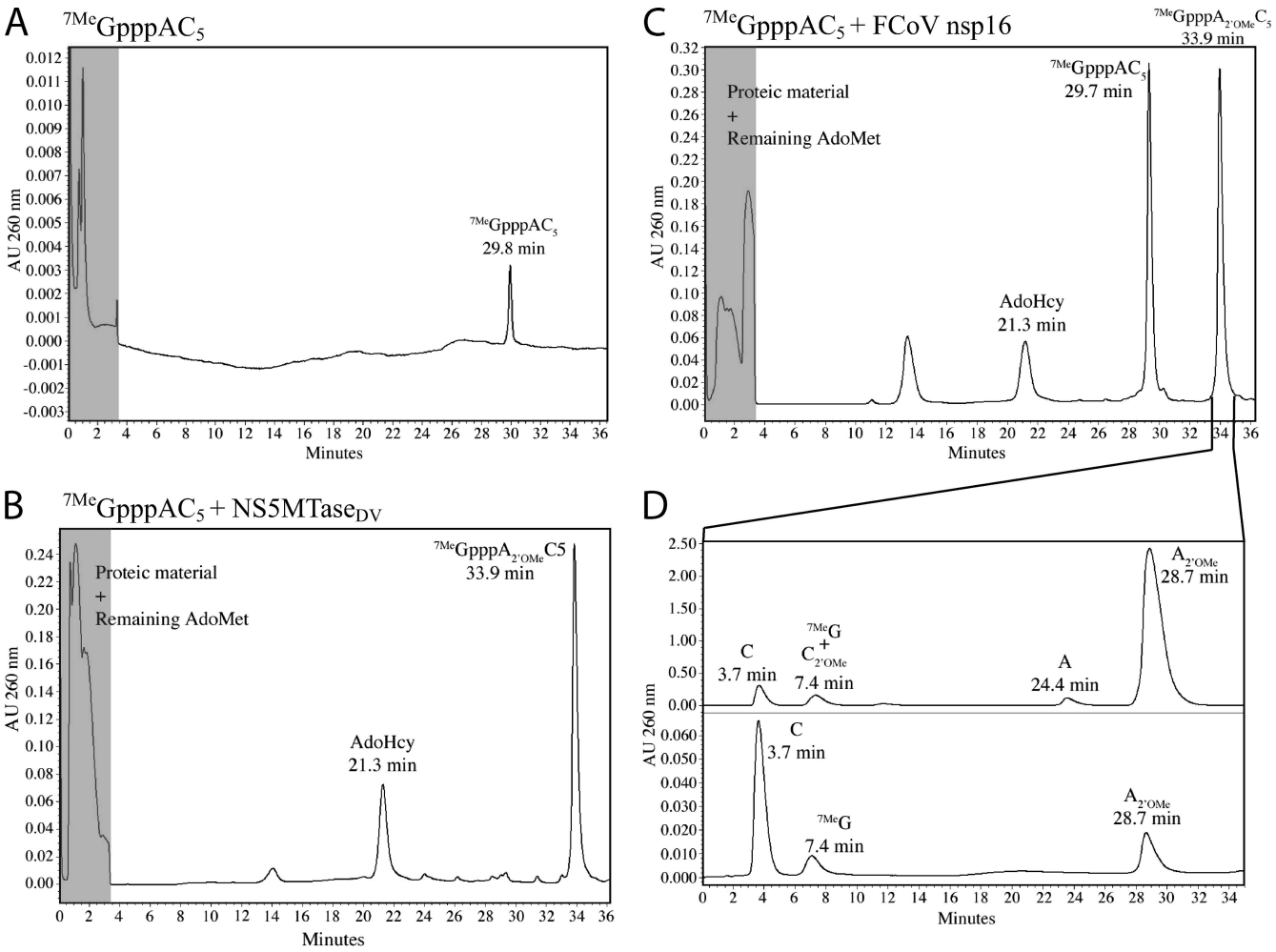

FIG. 3. FCoV nsp16 and NS5MTase$_{DV}$ methylate the 2′*O* position of the first transcribed nucleotide of the RNA. FCoV nsp16 or NS5MTase$_{DV}$ was incubated with ^{7Me}GpppAC$_5$ overnight. The crude reaction mixture was analyzed using reverse-phase HPLC. The first section (in gray) indicates the removal of proteic material and remaining AdoMet by on-line cleaning on the precolumn (see Material and Methods). The gradient started after 5 min at 100% eluent A, with an increase to 10% eluent B after 25 min, reaching 30% after 45 min. (A) HPLC profile of ^{7Me}GpppAC$_5$; (B) HPLC profile of ^{7Me}GpppAC$_5$ incubated overnight with NS5MTase$_{DV}$; and (C) HPLC profile of ^{7Me}GpppAC$_5$ incubated overnight with FCoV nsp16. The peak eluting at 33.9 min was collected and digested with a mixture of nucleotide pyrophosphatase, phosphodiesterase I, and calf intestine phosphatase. (D) HPLC chromatogram of digestion products analyzed without the on-line cleaning procedure (lower chromatogram) compared to a mixture of standard compounds (upper chromatogram). The gradient started after 5 min at 100% eluent A, with an increase to 10% eluent B after 25 min and to 30% after 45 min. Absorbances (AU) were measured at 260 nm.

^{7Me}G or a mixture of ^{7Me}G and C$_{2'OMe}$. We then performed a stoichiometric analysis of the cap components using the respective molar ratio corresponding to each nucleobase peak. The measured peak area (measured with the HPLC diode array detector) was divided by the molar extinction ε at 260 nm that corresponded to each nucleoside (C = 7,200, G = 11,500, ^{7Me}G = 10,100, and A$_{2'OMe}$ = 15,400). The relative molar ratios were found to be 0.82:1:6.2 for ^{7Me}G, A$_{2'OMe}$, and C, respectively. A cap-1 should yield ratios of 1:1:5, and a cap-2 in which ^{7Me}G comigrates with C$_{2'OMe}$ should yield 2:1:4. Taken together, these results demonstrate that FCoV nsp16 carries a 2′*O*-MTase activity that is capable of converting a cap-0 to a cap-1 RNA structure.

N7-methylated guanine of the cap structure is a binding determinant of FCoV nsp16. To gain insight into the mechanism of nsp16-mediated methylation, its binding to various substrates was analyzed. We conducted in vitro binding studies with small capped or uncapped RNAs of various lengths, with or without a methyl group at the N7 position. Using the T7 DNA primase system (58), short α-^{32}P-radiolabeled oligonucleotides were produced carrying ^{7Me}Gppp, Gppp, or ppp at their 5′ ends. These RNAs were incubated with either FCoV nsp16 or NS5MTase$_{DV}$ immobilized on Ni-NTA beads. After being incubated and washed, RNAs bound to the beads were resolved by PAGE and detected by autoradiography. As illustrated in Fig. 4A, empty control beads bound little of the tested RNAs. In contrast, specific RNAs were retained by the different MTase-carrying Ni-NTA beads. NS5MTase$_{DV}$ efficiently bound RNAs irrespective of their N7 methylation status (^{7Me}GpppAC$_{4-6}$ or GpppAC$_{4-6}$) but did not bind uncapped pppAC$_{2-6}$ RNA. In contrast, FCoV nsp16 exclusively bound capped RNAs that had a methyl at the cap N7 position (^{7Me}G

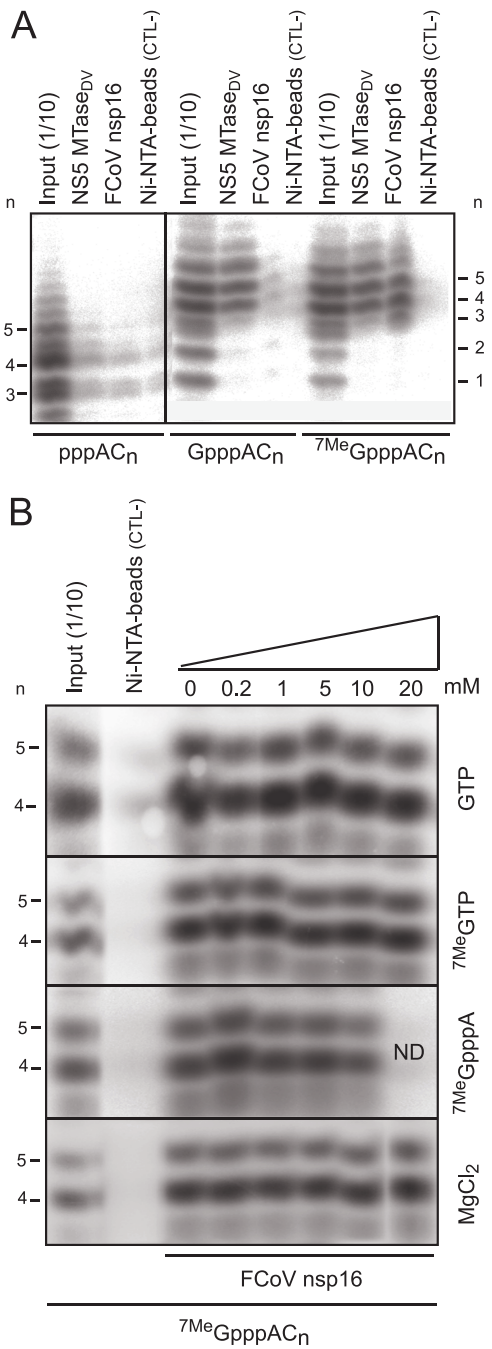

FIG. 4. Binding of noncapped RNAs or RNAs capped to FCoV nsp16 and NS5MTase$_{DV}$. Short ^{32}P-radiolabeled RNAs were incubated with equal amounts of FCoV nsp16 MTase and NS5MTase$_{DV}$, which previously had been immobilized on Sepharose beads. After three washes, the bound ^{32}P-labeled RNAs were separated by PAGE and detected by autoradiography. (A) PAGE analysis of pppAC$_n$, GpppAC$_n$, and ^{7Me}GpppAC$_n$ bound to FCoV nsp16 MTase, NS5MTase$_{DV}$, and empty Ni beads, which were used as negative controls (CTL−). The input (1/10) corresponded to 10% of the total radiolabeled RNA incubated with the MTase beads. (B) Binding of ^{7Me}GpppAC$_n$ to nsp16 MTase in the presence of increasing concentrations of $^{7Me±}$GTP, ^{7Me}GpppA, and Mg^{2+} cations. ND, not done, as the 20 mM point cannot be easily reached with commercially available ^{7Me}GpppA.

pppAC$_{3-6}$). Binding depended on RNA size, since capped RNAs with one or two 3′-terminal cytidines (^{7Me}GpppAC$_{1-2}$) did not bind efficiently to FCoV nsp16. Thus, requirements for efficient binding to nsp16 matched those favoring the MTase activity of the enzyme (compare Fig. 1B and 2C). We conclude that FCoV nsp16 specifically binds cap-0-bearing RNAs of at least 4 nucleotides in length. Both the RNA chain and the N7-methyl cap contribute to binding, but the presence of the latter is a prerequisite for binding. This substrate specificity is reminiscent of that of the VV 2′*O*-MTase VP39 (48) but quite different from that of the DV NS5MTase, which recognizes methylated and unmethylated capped RNA equally well (Fig. 4A and reference 19) and harbors both N7- and 2′*O*-MTase activities in a single peptide chain (66).

Since these results pinpointed nsp16 as a specific cap-0 binding protein, we sought to determine whether ^{7Me}GTP, GTP, or ^{7Me}GpppA could interfere with the binding of capped RNA, as previously shown for NS5MTase$_{DV}$ (20). To this end, we incubated nsp16–Ni-NTA beads with ^{7Me}GpppAC$_{3-6}$ and measured their binding capacity in the presence of an increasing concentration of GTP, ^{7Me}GTP, or ^{7Me}GpppA. Figure 4B shows that neither GTP nor ^{7Me}GTP (tested at up to 20 mM) had a clear effect on the interaction between nsp16 and RNA. The binding was slightly inhibited by ^{7Me}GpppA, starting at 10 mM. The binding of ^{7Me}GpppAC$_{3-6}$ also was not affected by an increasing concentration of Mg^{2+}, which was shown to stimulate nsp16 MTase activity (Fig. 2B). Thus, Mg^{2+} ions were not essential for substrate recognition, and ^{7Me}GTP and ^{7Me}GpppA were poor competitors for binding. The latter property was consistent with the fact that ^{7Me}GpppA could not efficiently serve as a substrate for nsp16. The VV VP39 2′*O*-MTase activity was not inhibited by ^{7Me}GTP or ^{7Me}GpppA (6). Interestingly, our nsp16 data contrast with the previously reported inhibition of the binding of NS5MTase$_{DV}$ to ^{7Me}GpppAC$_{3-6}$ or GpppAC$_{3-6}$ by GTP and ^{7Me}GTP (20). We conclude that the substrate binding site of the FCoV nsp16 MTase has a complex organization and interacts specifically with both cap-0 and nucleotides downstream of the RNA cap structure.

Inhibition of FCoV nsp16 2′*O*-MTase activity by AdoMet and GTP analogues. Since viral capping enzymes are interesting targets for antiviral therapy (61, 85, 86), we screened potential inhibitors of FCoV nsp16 MTase activity, starting with AdoMet/AdoHcy and GTP analogues, which previously were identified as inhibitors of AdoMet-dependent MTases (45, 51, 59–61). We first addressed whether GTP or ^{7Me}GTP could inhibit 2′*O*-MTase activity. For this purpose, nsp16 was incubated with ^{7Me}GpppAC$_5$ and [^{3}H]AdoMet in the presence of increasing ^{7Me}GTP or GTP concentrations, and the incorporation of label in methylated RNA was measured using the filter binding assay. Surprisingly, although GTP and ^{7Me}GTP were unable to block the binding of nsp16 to its substrate even at 20 mM (Fig. 4B), we observed that both nucleotides inhibited MTase activity significantly, yielding IC$_{50}$ values of 1.51 ± 0.11 and 1.25 ± 0.12 mM, respectively (Fig. 5A). This observation suggests that these nucleotides do not act purely as competitive inhibitors of substrate binding. They might interfere with the binding of a specific part of the RNA substrate while leaving the overall binding unchanged.

Using the same assay, we next tested whether FCoV nsp16 was inhibited by a fixed (100 μM) concentration of different

GTP analogues, AdoMet, and the AdoHcy by-product of the methylation reaction (Fig. 5B). All tested compounds, including AdoHcy, which is known to be a potent inhibitor of the MTase family (6, 61), proved to be poor inhibitors of the MTase activity. The IC_{50} of AdoHcy was 144 μM (Fig. 5C), approximately 100-fold higher than the concentrations commonly required to inhibit other MTases (6, 61). Likewise, sinefungin, which previously was shown to be a potent inhibitor of the MTases of Newcastle disease virus and VV (IC_{50} values of 150 and 75 nM, respectively [60]), was found to be a very poor inhibitor for FCoV nsp16. Thus, we conclude that nsp16, unlike its distant viral homologues, can efficiently discriminate AdoMet and its analogues, suggesting that although various AdoMet-dependent MTases share a similar structural organization (see below), nsp16 evolved a specific variant of the conserved AdoMet binding site.

Identification of key residues for FCoV nsp16 2′*O*-MTase activity and substrate binding. To identify residues involved in catalysis and substrate binding, we engineered and characterized a set of FCoV nsp16 point mutants. The positions to be mutated were selected using a comparative analysis of nsp16 and other, better characterized MTase homologues. We started from a structure-based sequence alignment of four RNA 2′*O*-MTases with known tertiary structures. These enzymes of viral and cellular origin were aligned with nsp16 of SARS-CoV and FCoV, and for the latter a secondary structure prediction was generated (Fig. 6A). Due to the considerable divergence of the protein sequences used, only limited conservation is evident in the alignment, in particular in regions corresponding to the MTase core, which is structurally conserved among AdoMet-dependent MTases (14, 52). In line with the original analysis of CoV nsp16 (76, 82), four out of six invariant residues in the alignment correspond to the K-D-K-E catalytic tetrad of RNA 2′*O*-MTases (12, 19). These four residues (K45, D129, K169, and E202 in FCoV) were selected for mutagenesis. To identify other potentially important residues, the tertiary organization of the FCoV nsp16 MTase core was modeled through different Web servers (see Materials and Methods). Although the VP39 and FCoV nsp16 MTases share the same binding specificity for cap-0 structures, they were found to be too divergent for any server to produce a meaningful nsp16 model. The closest template proposed by several servers was the rRNA 2′*O*-MTase FtsJ (11), which therefore was used to model FCoV nsp16 using HHpred (77). An inspection of the final model (Fig. 6B) of the MTase core of nsp16 (residues K45 to G221) and other MTase structures (Fig. 6C and D) showed that in all structures but that of VP39, the spatial equivalent of FCoV nsp16 residue D113 (conserved in CoV nsp16) is also an Asp residue (11, 19), which is located close to the AdoMet. Therefore, residue D113 of FCoV nsp16 was selected for mutagenesis.

The identification of residues that might be involved in substrate binding was less straightforward. Our starting point was the observation that VV VP39 shares with nsp16 a high specificity for the cap-0 structure. In the structure of VP39 complexed with a ^{7Me}G-capped RNA (Fig. 6C) (33), the methylated base is stacked between two aromatic side chains (Y22 and F180) (Fig. 6A and C). Moreover, in VP39 the methyl group is in contact with residue Y204 (Fig. 6A and C) via van der Waals interactions (33, 64). Finally, the carboxyl groups of

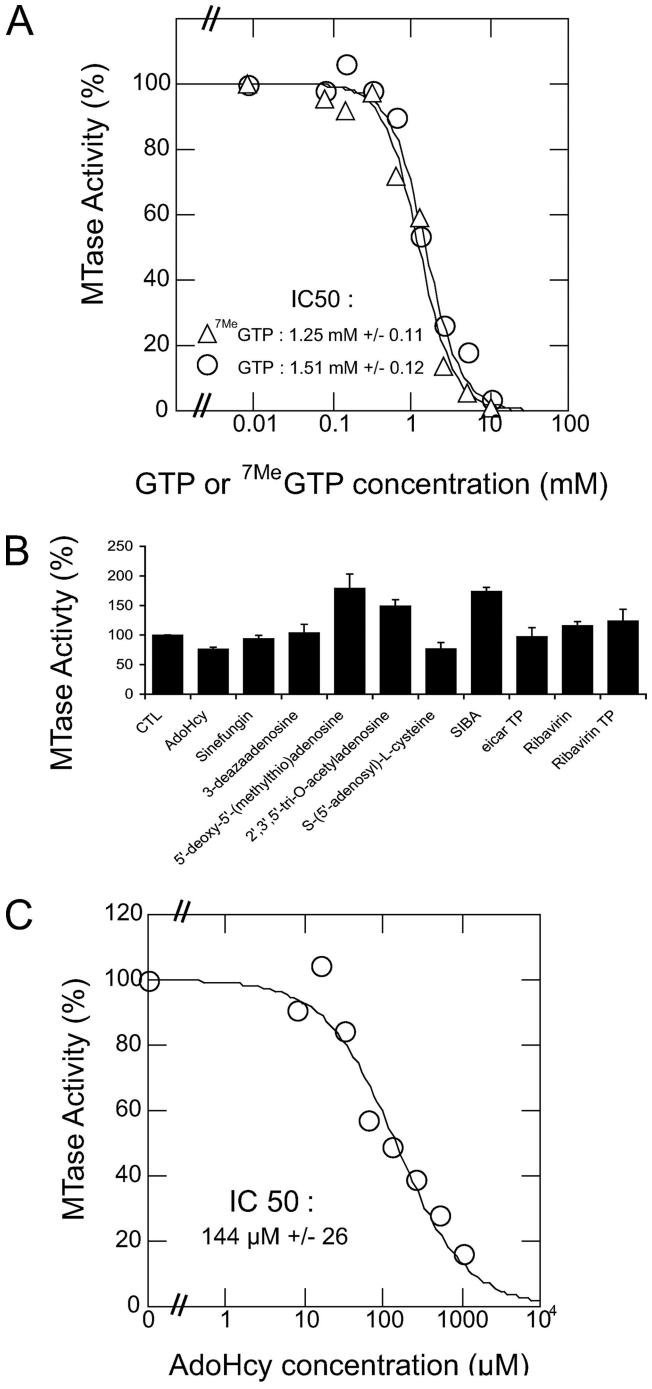

FIG. 5. Inhibition of FCoV nsp16 MTase activity by GTP and AdoMet analogues. The nsp16 MTase was incubated with [^{3}H]AdoMet and ^{7Me}GpppAC$_5$ in the presence of various potential inhibitors. MTase activity was determined by measuring the radioactivity associated with the RNA substrates using filter binding assays. (A) Inhibition curve of nsp16 activity by GTP (○) and ^{7Me}GTP (△). The nsp16 activity obtained in the absence of inhibitors was set to 100%. The standard deviations from three independent experiments are shown, and the IC_{50} value was calculated as indicated in Materials and Methods. (B) Inhibition by various AdoMet analogues at a concentration of 100 μM. Activity of 100% corresponds to the nsp16 activity on the ^{7Me}GpppAC$_5$ substrate in the absence of inhibition. CTL, control. SIBA, 5′-deoxy-5′-S-isobutylthioadenosine; TP, triphosphate. (C) Inhibition curve of FCoV nsp16 activity by the reaction product (AdoHcy). The IC_{50} values were determined as described for panel A.

residues D182 and E233 form hydrogen bonds to the NH and NH2 of the guanosine in VP39. Most of these residues are located in regions for which the counterparts in the FCoV nsp16 could not be modeled by HHpred. The only exception was the loop region immediately downstream of β-strand 6, in which we selected residues F173 and W175 for mutagenesis, as they are a putative counterpart of VP39 F180 (Fig. 6B). To probe for cap binding residues in the most divergent N- and C-terminal regions, we limited our selection to residues conserved in CoV that are physicochemically similar to those involved in substrate recognition in VP39. Aromatic residues W4, Y14, and Y29 in the nsp16 N terminus were selected as putative equivalents of Y22 and Y204 in VP39 and residues D221 and D247 in the nsp16 C terminus (Fig. 6A) as candidates for the role of E233 in VP39.

Of the 12 nsp16 mutants engineered, all but W175A were expressed at a level sufficient to allow the purification of the enzyme by our two-step procedure. Consequently, W175A could not be analyzed further. Both their $^{7Me}GpppAC_5$ binding capacity and their MTase activity on capped RNA oligonucleotides ($^{7Me}GpppAC_5$ and $GpppAC_5$) were compared to those of the wt control (Fig. 7). For none of the mutants was there a change in the dependence on a N7-methylated cap or the selectivity compared to that of an unmethylated cap (Fig. 7A). The MTase activity was abolished or severely reduced by all mutations affecting the putative K-D-K-E catalytic tetrad, supporting their structure-based assignment as being functionally essential (Fig. 6A). One of these mutations (K45A) also abolished the binding of capped RNA (Fig. 7C), while mutations at three other positions reduced it to 20 to 50% of the level observed for the wt protein. This result indicated that K45, and possibly other catalytic residues, contribute to the specific recognition of cap-0 RNA. In the case of D113, which may be part of the predicted AdoMet binding pocket, replacement by Ala reduced 2′*O*-MTase activity to about 10% of the wt level without an apparent effect on substrate binding. In contrast, Ala replacements of the aromatic residues located in the N-terminal subdomain (Y14 and Y29) and downstream of β-strand 6 (F173) also reduced the binding of nsp16 to its substrate to 10 to 20% of the wt level (Fig. 7C). The effects on the MTase activity varied considerably, from complete inhibition (Y29A) to a modest 50% reduction (F173A) or a minor ~18% drop (Y14A). Mutations W4A, D221A, and D247A formed a group in which the effect of replacement by Ala on both RNA binding and 2′*O*-MTase activity was comparable, ranging from no change to 55% inhibition at most.

We conclude that the FCoV nsp16 2′*O*-MTase employs the canonical K-D-K-E catalytic tetrad that consists of K45, D129, K169, and E202. Residue D113 also may contribute to catalysis but not to RNA binding. Two residues (K45 and Y29) for which mutagenesis severely compromised both MTase activity and substrate binding may be involved in both substrate recognition and catalysis or, alternatively, only in the specific recognition of cap-0 RNA.

DISCUSSION

Upon CoV infection, replicases ORF1a and ORF1b of the positive-strand RNA genome are translated, presumably by using a cap-dependent mechanism (44, 80). Although the cap is expected to be essential for ribosome binding and efficient viral mRNA translation (24, 75), the RNA capping mechanism of CoV is essentially uncharacterized. It supposedly involves four enzymatic activities (24), including an RTPase (40, 41), a GTase, and two MTase activities.

The ORF1b-encoded replicase subunits of CoV (nsp12 to nsp16) include five RNA-processing enzymes that have uniquely segregated in the genomes of CoV and other large nidoviruses (28, 76). In recent years, the activities of four of these enzymes, but not the nsp16 MTase, were characterized for one or more CoV. In this report, we document the MTase activity of nsp16, the C-terminal subunit of the CoV replicase. FCoV nsp16 specifically and selectively binds capped RNAs of 3 to 6 nucleotides in length that carry a methyl group at the N7 position of the guanosine cap, a chemical entity known as the cap-0 structure ($^{7Me}GpppAC_{3-6}$). FCoV nsp16 catalyzes the transfer of a methyl group from the AdoMet donor to short capped RNAs, but only when they carry a methyl group at the N7-guanine position.

Different 2′*O*-MTases were reported to target either the first (71, 72) or subsequent transcribed nucleotides of capped RNAs (32). We have identified the methylation position using an enzymatic digestion of the reaction products in conjunction with HPLC analysis. The latter demonstrated that the nsp16 MTase targets the 2′*O* position of the first nucleotide, thus converting $^{7Me}GpppAC_n$ into $^{7Me}GpppA_{2'OMe}C_n$. Thus, FCoV nsp16 belongs to the family of AdoMet-dependent mRNA cap 2′*O*-MTases that specifically methylates the first endogenous nucleotide of the cap-0 structure to produce a cap-1 structure. These findings support the proposed involvement of nsp16 in CoV translational control (76, 82) and the suggestion that CoV mRNAs carry a cap structure (44, 80). A more extensive analysis of nsp16 is required to verify whether this enzyme also methylates other nucleotides in virus and/or cellular RNAs to regulate other processes in cooperation with virus RNA-processing enzymes, as proposed previously (76). With these findings, two of the four cap-forming enzyme functions now have been reported for CoV: an RTPase activity was mapped to the multifunctional nsp13 helicase protein of HCoV 229E (41) and SARS-CoV (40) and the 2′*O*-MTase activity reported here for FCoV nsp16.

Our finding that the FCoV nsp16 2′*O*-MTase strongly prefers substrates carrying a cap-0 structure over those that have a nonmethylated cap indicates that cap maturation in CoV follows the canonical order of methylation steps that have been described for other biological systems. This will have to be compared to the cap methylation recently documented for flaviviruses, in which the NS5 MTase recognizes both methylated and nonmethylated cap structures (this work and reference 20) and catalyzes the methylation of both the N7 position of the guanine as well as the 2′*O* position of the nucleotide ribose (66, 86). It is possible that nsp16 also possesses N7-guanine MTase activity in the presence of longer substrates, e.g., RNA sequences and/or structures specific for the 5′-untranslated region of the viral genome. For example, the specificity of the West Nile virus (WNV) NS5MTase for WNV-specific RNA sequences recently was reported (16, 66). If such a dependence exists in the case of CoV, RNA sequences downstream of the cap structure might represent regulatory elements inducing specific N7 or 2′*O*-methylation events.

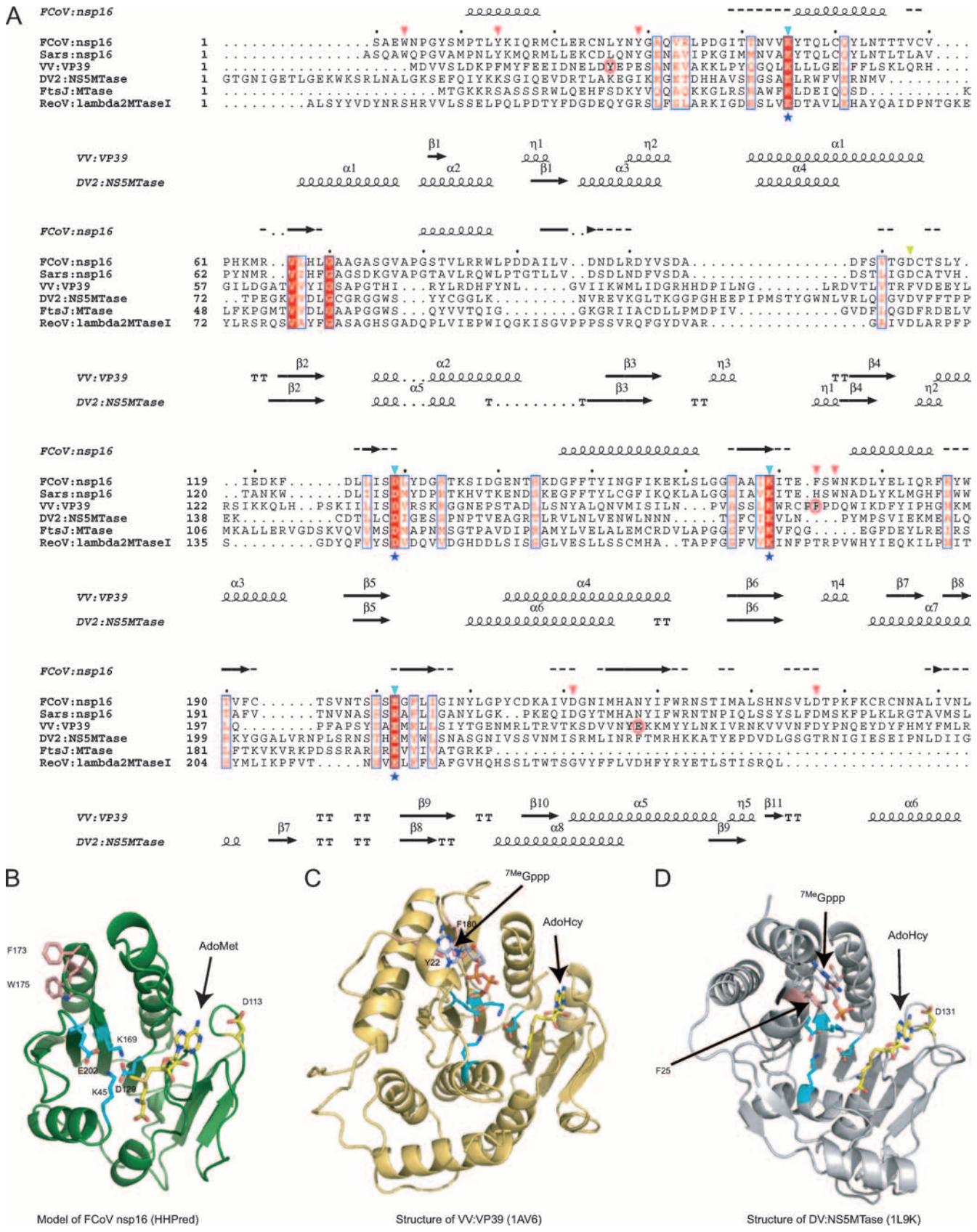

FIG. 6. Comparative analysis of viral MTases. (A) Structure-based alignment of the MTase core domain of FCoV nsp16 with SARS-CoV nsp16 (82), the VV mRNA MTase VP39 (34), $NS5MTase_{DV}$ (19), the rRNA MTase FtsJ (11), the C-terminal rRNA MTase domain of Mj0697 (83), and

Residues potentially involved in substrate binding and the methyl transfer reaction were probed by mutagenesis. In addition to the catalytic tetrad K-D-K-E, residue D113 of the AdoMet binding site and residue Y29 are essential for 2′*O*-MTase activity. Similar results were reported recently for the WNV MTase. Using alanine-scanning mutagenesis, it was shown that its K-D_{146}-K-E catalytic tetrad is essential for 2′*O* methylation activity, whereas the N7-MTase activity depends mainly on D_{146} (86). The catalytic residues are adequately positioned in the three-dimensional structural model of FCoV nsp16 (Fig. 6B). Interestingly, we noted that some residues of the catalytic tetrad also are important for the efficient binding of the capped RNA substrate. This observation suggests that the binding of cap RNA involves multiple contact regions. Accordingly, binding assays revealed that a shorter cap-1-containing RNA, ^{7Me}GpppAC$_{1-2}$, did not bind to FCoV nsp16, whereas longer molecules did. The more efficient binding of longer RNAs suggests that the presence of nucleotides downstream from the cap binding site is necessary to stabilize the interaction between FCoV nsp16 and its RNA substrate. This also was confirmed by the poor inhibition of binding observed in the presence of increasing concentrations of ^{7Me}GpppA cap analogue and ^{7Me}GTP. In particular, the K45A substitution was quite spectacular in terms of its effect on both MTase activity and RNA binding. A single nsp16 point mutation abolishing RNA binding is remarkable. Indeed, ^{7Me}GpppAC$_5$ should interact with many residues of the enzyme, each contributing moderately to RNA binding. Could K45 be an essential residue responsible for specific cap recognition? The superimposition of the VP39 and nsp16 models shows that the methylated guanosine cap binding site is remote from K45 (Fig. 6B and C), suggesting that K45A has a drastic indirect effect on the putative RNA binding groove but not a direct effect on the binding of the methylated cap. In contrast, the fact that D113A did not influence substrate binding is consistent with its specific position within the putative AdoMet-binding site. The corresponding residue in NS5MTase$_{DV}$ is located on the side of the AdoMet cofactor, not adjacent to the positively charged, putative RNA-binding groove (20).

Our mutagenesis study confirmed a contribution of at least one aromatic amino acid to the specificity of methylated cap recognition. Since Y29A abolished both cap-0 recognition and the 2′*O*-MTase activity of FCoV nsp16, we propose that this residue plays an essential role in specific cap recognition through a stacking interaction with cap-0 RNA, which in turn might allow the correct positioning of capped RNA into the catalytic site. Unfortunately, Y29 could not be visualized in the structural model. In contrast, the Y14A and F173A replacements did not reduce 2′*O*-MTase activity as extensively as they inhibited RNA binding. This observation may be explained by the stringent washing conditions in our binding assay and suggests that both residues contribute to cap recognition. The cap binding site of the VV VP39 MTase previously was shown to depend on two aromatic side chains (Y22 and F180) that are necessary to recognize the cap-0 structure by stacking interactions (35), and the replacement of F180 drastically inhibited 2′*O*-MTase activity (36). If we assume that a cap binding site is located in the same area in both FCoV nsp16 and VV VP39, F173 is adequately positioned in the three-dimensional model of nsp16 (Fig. 6B) to bind to the cap-0 structure. Therefore, we hypothesize that FCoV nsp16 stacks the methylated guanine moiety of the cap-0 structure between two aromatic residues, similarly to what was found for VV VP39 and the mammalian cap binding translation initiation factor eIF4E (32, 35, 64). As the most likely candidates for this role, we propose residues Y29 and F173 without formally excluding Y14.

Virus-encoded RNA cap 2′*O*-MTase activities previously have been identified for various other virus genera, such as poxviruses (VP39 [71, 72]), the double-stranded reoviruses (50, 65), minus-strand ssRNA viruses such as VSV (47), and positive-strand ssRNA viruses like flaviviruses (NS5MTase [19, 58, 86]). The exact role of mRNA cap 2′*O*-methylation in the virus life cycle is still an open question. It is likely that this function confers a replicative advantage on the virus, since 2′*O*-MTases are widely conserved among viruses that have cap-bearing genomes and/or mRNAs. For the WNV MTase, it has been shown that mutations abolishing the N7 and/or 2′*O*-MTase activity have a detrimental effect on the replication of a luciferase-expressing RNA replicon (66). In contrast, when viral replication was tested directly, a substitution inactivating the N7-MTase activity substantially attenuated replication, whereas 2′*O*-MTase knockouts had more moderate effects (66, 86). These observations suggest that compounds specifically inhibiting cap-methylating enzymes, either N7-MTase or 2′*O*-MTase or both, could act as potent antiviral agents. Accordingly, a series of AdoMet analogues containing modifications of the nucleoside moiety showed potent and selective antiviral activity against herpes simplex virus, VV, and VSV (5, 61). In

the mRNA MTase domain I of reovirus (Reov) λ2 (67). The alignment was generated manually using Seaview (25) and was presented with the ESPript program (30). The positions of conserved residues are highlighted by a red background, and the regions outlined in blue indicate high sequence similarity (>70%). The secondary-structure elements of the VP39 and NS5Mtase$_{DV}$ structures and their names are given below the alignment. The predicted FCoV nsp16 secondary structure generated by the PSIPRED protein structure prediction server (10) is indicated above the alignment. The position of the mutations characterized in this study are indicated by triangles above the FCoV nsp16 sequence: salmon triangles for the putative cap-0 binding site, light blue/turquoise for the catalytic site, and yellow for the AdoMet binding site. The conserved catalytic active-site residues K-D-K-E of RNA 2′*O*-MTases are annotated by blue stars, and the VP39 residues participating in cap recognition are indicated with salmon circles. Also shown are the structural comparative analyses of viral Mtases. (B) Ribbon representation of the FCoV nsp16 model as generated on the basis of the structure of rRNA 2′*O*-MTase FtsJ (see Materials and Methods). AdoMet was placed by the superimposition of the FCoV nsp16 model and the structure of rRNA 2′*O*-MTase FtsJ in complex with the cofactor. Structures of VP39 (PDB ID 1AV6) (C) and NS5MTase$_{DV}$ (PDB ID 1L9K) (D) also are shown. A yellow stick representation is used to show AdoMet and the reaction product AdoHcy, with oxygen in red and nitrogen in blue. The side chains and carbon backbone of conserved catalytic residues K-D-K-E are represented by sticks in blue/turquoise (K45 was manually added in the FCoV nsp16 model). The lateral chain of nsp16 D113, which is involved in AdoMet binding, is shown in yellow. The VP39 side chains of residues involved in the binding of the ^{7Me}G cap are represented in salmon, and the cap analogues are in light gray.

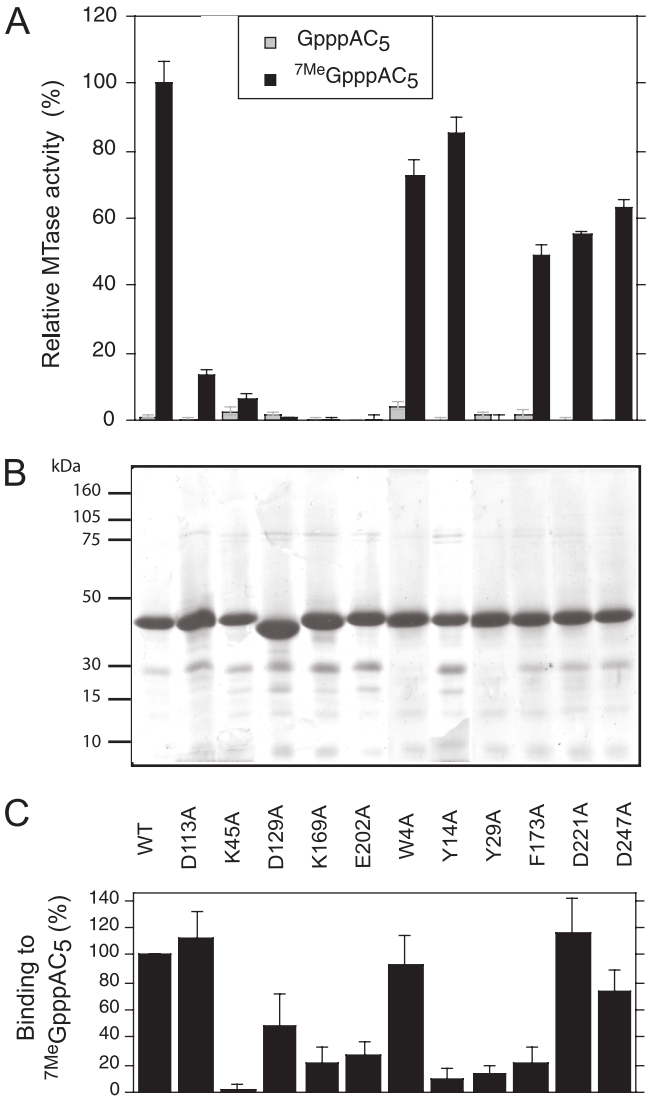

FIG. 7. Alanine-scanning mutagenesis of the FCoV nsp16. Activity and substrate binding of FCoV nsp16 mutants. (A) Equal amounts of the different nsp16 mutants were incubated with $GpppAC_5$ and $^{7Me}GpppAC_5$ in the presence of [^{3}H]AdoMet. The methyl transfer to the RNA substrate was monitored during a 240-min time course experiment and detected using a filter binding assay that measured the amount of radioactivity, in cpm, that was transferred to the RNA substrates. MTase activity of 100% was arbitrarily attributed to the wt nsp16 activity when using the $^{7Me}GpppAC_5$ substrate. The bar graph presents the results of three independent experiments. (B) The purified nsp16 mutants after separation on SDS–12% Page and Coomassie blue staining. (C) The binding of $^{7Me}GpppAC_5$ to nsp16 mutants was determined as described in the legend to Fig. 4. Binding data were normalized (100% corresponds to $^{7Me}GpppAC_5$ bound to wt nsp16).

this study, we tested whether some of these AdoMet analogues (e.g., sinefungin, which has an IC_{50} of 39 nM for VV VP39 [60]) would block nsp16 MTase activity, but all of the molecules tested proved to be weak inhibitors.

Our observations suggest that the CoV nsp16 MTase is a unique enzyme: it shares its structural organization and specificity for the cap-0 structure with VV VP39, but the divergence of the structurally conserved AdoHcy binding site results in unusually weak inhibition profiles for AdoMet analogues. Furthermore, nsp16 has evolved a unique substrate binding site that cooperates with the canonical catalytic tetrad that is conserved in other 2′*O*-MTases to recruit its substrate. Finally, despite the inability of GTP and ^{7Me}GTP to block cap-0 binding, both nucleotides inhibit FCoV nsp16 activity at similar concentrations, suggesting that the nucleotide binding site is distinct from the site binding the methylated cap. Further functional and structural exploration of FCoV nsp16 will be necessary to define this putative binding site, which is of potential interest for inhibitor design.

ACKNOWLEDGMENTS

We thank Stuart Siddell (University of Bristol, United Kingdom) for kindly providing FCoV. A.E.G. acknowledges his collaboration with John Ziebuhr on the MTase of CoV. We thank Karen Dalle, Violaine Lantez, Marilyne Blemont, Séverine Blanc, Christophe Flaudrops, and Linda Boomaars-van der Zanden for excellent technical assistance and Cecile Bussetta for help in model building. We gratefully thank Aron Shatkin for the kind gift of the hN7-MTase cDNA clone.

This work was supported by the VIZIER integrated project (LSHG-CT-2004-511960) of the European Union 6th Framework, by the Euro-Asian SARS-DTV Network (SP22-CT-2004-511064) from the European Commission on Specific Research and Technological Development Program Integrating and Strengthening the European Research Area, and in part by grants from the Direction Générale de l'Armement (contract no. 07co404) and the French Ministry of Research 2007 (program Maladies Infectieuses et Émergentes).

REFERENCES

1. **Addie, D. D., and O. Jarrett.** 2001. Use of a reverse-transcriptase polymerase chain reaction for monitoring the shedding of feline coronavirus by healthy cats. Vet. Rec. **148:**649–653.
2. **Ahola, T., and L. Kaariainen.** 1995. Reaction in alphavirus mRNA capping: formation of a covalent complex of nonstructural protein nsP1 with 7-methyl-GMP. Proc. Natl. Acad. Sci. USA **92:**507–511.
3. **Almazán, F., M. L. Dediego, C. Galan, D. Escors, E. Alvarez, J. Ortego, I. Sola, S. Zuniga, S. Alonso, J. L. Moreno, A. Nogales, C. Capiscol, and L. Enjuanes.** 2006. Construction of a severe acute respiratory syndrome coronavirus infectious cDNA clone and a replicon to study coronavirus RNA synthesis. J. Virol. **80:**10900–10906.
4. **Baker, S. C., K. Yokomori, S. Dong, R. Carlisle, A. E. Gorbalenya, E. V. Koonin, and M. M. Lai.** 1993. Identification of the catalytic sites of a papain-like cysteine proteinase of murine coronavirus. J. Virol. **67:**6056–6063.
5. **Balzarini, J., E. De Clercq, P. Serafinowski, E. Dorland, and K. R. Harrap.** 1992. Synthesis and antiviral activity of some new S-adenosyl-L-homocysteine derivatives. J. Med. Chem. **35:**4576–4583.
6. **Barbosa, E., and B. Moss.** 1978. mRNA(nucleoside-2′-)-methyltransferase from vaccinia virus. Characteristics and substrate specificity. J. Biol. Chem. **253:**7698–7702.
7. **Bartelma, G., and R. Padmanabhan.** 2002. Expression, purification, and characterization of the RNA 5′-triphosphatase activity of dengue virus type 2 nonstructural protein 3. Virology **299:**122–132.
8. **Benarroch, D., B. Selisko, G. A. Locatelli, G. Maga, J. L. Romette, and B. Canard.** 2004. The RNA helicase, nucleotide 5′-triphosphatase, and RNA 5′-triphosphatase activities of Dengue virus protein NS3 are $Mg2^+$-dependent and require a functional Walker B motif in the helicase catalytic core. Virology **328:**208–218.
9. **Brierley, I., P. Digard, and S. C. Inglis.** 1989. Characterization of an efficient coronavirus ribosomal frameshifting signal: requirement for an RNA pseudoknot. Cell **57:**537–547.
10. **Bryson, K., L. J. McGuffin, R. L. Marsden, J. J. Ward, J. S. Sodhi, and D. T. Jones.** 2005. Protein structure prediction servers at University College London. Nucleic Acids Res. **33:**W36–W38.
11. **Bügl, H., E. B. Fauman, B. L. Staker, F. Zheng, S. R. Kushner, M. A. Saper, J. C. Bardwell, and U. Jakob.** 2000. RNA methylation under heat shock control. Mol. Cell **6:**349–360.
12. **Bujnicki, J. M., and L. Rychlewski.** 2002. In silico identification, structure prediction and phylogenetic analysis of the 2′-O-ribose (cap 1) methyltransferase domain in the large structural protein of ssRNA negative-strand viruses. Protein Eng. **15:**101–108.
13. **Cheng, A., W. Zhang, Y. Xie, W. Jiang, E. Arnold, S. G. Sarafianos, and J. Ding.** 2005. Expression, purification, and characterization of SARS coronavirus RNA polymerase. Virology **335:**165–176.

14. **Cheng, X., and R. Blumentahal.** 1999. S-adenosylmethionine-dependent methyltranferases: structures and functions. World Scientific Publishing Co., Ltd., Hackensack, NJ.
15. **DeLean, A., P. J. Munson, and D. Rodbard.** 1978. Simultaneous analysis of families of sigmoidal curves: application to bioassay, radioligand assay, and physiological dose-response curves. Am. J. Physiol. **235:**E97–E102.
16. **Dong, H., D. Ray, S. Ren, B. Zhang, F. Puig-Basagoiti, Y. Takagi, C. K. Ho, H. Li, and P. Y. Shi.** 2007. Distinct RNA elements confer specificity to flavivirus RNA cap methylation events. J. Virol. **81:**4412–4421.
17. **Drosten, C., S. Gunther, W. Preiser, S. van der Werf, H. R. Brodt, S. Becker, H. Rabenau, M. Panning, L. Kolesnikova, R. A. Fouchier, A. Berger, A. M. Burguiere, J. Cinatl, M. Eickmann, N. Escriou, K. Grywna, S. Kramme, J. C. Manuguerra, S. Muller, V. Rickerts, M. Sturmer, S. Vieth, H. D. Klenk, A. D. Osterhaus, H. Schmitz, and H. W. Doerr.** 2003. Identification of a novel coronavirus in patients with severe acute respiratory syndrome. N. Engl. J. Med. **348:**1967–1976.
18. **Dye, C., and S. G. Siddell.** 2005. Genomic RNA sequence of feline coronavirus strain FIPV WSU-79/1146. J. Gen. Virol. **86:**2249–2253.
19. **Egloff, M. P., D. Benarroch, B. Selisko, J. L. Romette, and B. Canard.** 2002. An RNA cap (nucleoside-2′-O-)-methyltransferase in the flavivirus RNA polymerase NS5: crystal structure and functional characterization. EMBO J. **21:**2757–2768.
20. **Egloff, M. P., E. Decroly, H. Malet, B. Selisko, D. Benarroch, F. Ferron, and B. Canard.** 2007. Structural and functional analysis of methylation and 5′-RNA sequence requirements of short capped RNAs by the methyltransferase domain of dengue virus NS5. J. Mol. Biol. **372:**723–736.
21. **Ensinger, M. J., S. A. Martin, E. Paoletti, and B. Moss.** 1975. Modification of the 5′-terminus of mRNA by soluble guanylyl and methyl transferases from vaccinia virus. Proc. Natl. Acad. Sci. USA **72:**2525–2529.
22. **Feder, M., J. Pas, L. S. Wyrwicz, and J. M. Bujnicki.** 2003. Molecular phylogenetics of the RrmJ/fibrillarin superfamily of ribose 2′-O-methyltransferases. Gene **302:**129–138.
23. **Ferron, F., S. Longhi, B. Henrissat, and B. Canard.** 2002. Viral RNA-polymerases—a predicted 2′-O-ribose methyltransferase domain shared by all Mononegavirales. Trends Biochem. Sci. **27:**222–224.
24. **Furuichi, Y., and A. J. Shatkin.** 2000. Viral and cellular mRNA capping: past and prospects. Adv. Virus Res. **55:**135–184.
25. **Galtier, N., M. Gouy, and C. Gautier.** 1996. SEAVIEW and PHYLO_WIN: two graphic tools for sequence alignment and molecular phylogeny. Comput. Appl. Biosci. **12:**543–548.
26. **Ginalski, K., A. Godzik, and L. Rychlewski.** 2006. Novel SARS unique AdoMet-dependent methyltransferase. Cell Cycle **5:**2414–2416.
27. **Golovanov, A. P., G. M. Hautbergue, S. A. Wilson, and L. Y. Lian.** 2004. A simple method for improving protein solubility and long-term stability. J. Am. Chem. Soc. **126:**8933–8939.
28. **Gorbalenya, A. E., L. Enjuanes, J. Ziebuhr, and E. J. Snijder.** 2006. Nidovirales: evolving the largest RNA virus genome. Virus Res. **117:**17–37.
29. **Gorbalenya, A. E., E. J. Snijder, and W. J. Spaan.** 2004. Severe acute respiratory syndrome coronavirus phylogeny: toward consensus. J. Virol. **78:**7863–7866.
30. **Gouet, P., E. Courcelle, D. I. Stuart, and F. Metoz.** 1999. ESPript: analysis of multiple sequence alignments in PostScript. Bioinformatics **15:**305–308.
31. **Guo, P. X., and B. Moss.** 1990. Interaction and mutual stabilization of the two subunits of vaccinia virus mRNA capping enzyme coexpressed in Escherichia coli. Proc. Natl. Acad. Sci. USA **87:**4023–4027.
32. **Hall, M. P., and C. K. Ho.** 2006. Functional characterization of a 48 kDa Trypanosoma brucei cap 2 RNA methyltransferase. Nucleic Acids Res. **34:** 5594–5602.
33. **Hodel, A. E., P. D. Gershon, and F. A. Quiocho.** 1998. Structural basis for sequence-nonspecific recognition of 5′-capped mRNA by a cap-modifying enzyme. Mol. Cell **1:**443–447.
34. **Hodel, A. E., P. D. Gershon, X. Shi, and F. A. Quiocho.** 1996. The 1.85 A structure of vaccinia protein VP39: a bifunctional enzyme that participates in the modification of both mRNA ends. Cell **85:**247–256.
35. **Hu, G., P. D. Gershon, A. E. Hodel, and F. A. Quiocho.** 1999. mRNA cap recognition: dominant role of enhanced stacking interactions between methylated bases and protein aromatic side chains. Proc. Natl. Acad. Sci. USA **96:**7149–7154.
36. **Hu, G., A. Oguro, C. Li, P. D. Gershon, and F. A. Quiocho.** 2002. The "cap-binding slot" of an mRNA cap-binding protein: quantitative effects of aromatic side chain choice in the double-stacking sandwich with cap. Biochemistry **41:**7677–7687.
37. **Imbert, I., J. C. Guillemot, J. M. Bourhis, C. Bussetta, B. Coutard, M. P. Egloff, F. Ferron, A. E. Gorbalenya, and B. Canard.** 2006. A second, non-canonical RNA-dependent RNA polymerase in SARS coronavirus. EMBO J. **25:**4933–4942.
38. **Imbert, I., E. J. Snijder, M. Dimitrova, J. C. Guillemot, P. Lecine, and B. Canard.** 2008. The SARS-coronavirus PLnc domain of nsp3 as a replication/transcription scaffolding protein. Virus Res. **133:**136–148.
39. **Ivanov, K. A., T. Hertzig, M. Rozanov, S. Bayer, V. Thiel, A. E. Gorbalenya, and J. Ziebuhr.** 2004. Major genetic marker of nidoviruses encodes a replicative endoribonuclease. Proc. Natl. Acad. Sci. USA **101:**12694–12699.
40. **Ivanov, K. A., V. Thiel, J. C. Dobbe, Y. van der Meer, E. J. Snijder, and J. Ziebuhr.** 2004. Multiple enzymatic activities associated with severe acute respiratory syndrome coronavirus helicase. J. Virol. **78:**5619–5632.
41. **Ivanov, K. A., and J. Ziebuhr.** 2004. Human coronavirus 229E nonstructural protein 13: characterization of duplex-unwinding, nucleoside triphosphatase, and RNA 5′-triphosphatase activities. J. Virol. **78:**7833–7838.
42. **Jeffery, D. R., and J. A. Roth.** 1987. Kinetic reaction mechanism for magnesium binding to membrane-bound and soluble catechol O-methyltransferase. Biochemistry **26:**2955–2958.
43. **Ksiazek, T. G., D. Erdman, C. S. Goldsmith, S. R. Zaki, T. Peret, S. Emery, S. Tong, C. Urbani, J. A. Comer, W. Lim, P. E. Rollin, S. F. Dowell, A. E. Ling, C. D. Humphrey, W. J. Shieh, J. Guarner, C. D. Paddock, P. Rota, B. Fields, J. DeRisi, J. Y. Yang, N. Cox, J. M. Hughes, J. W. LeDuc, W. J. Bellini, and L. J. Anderson.** 2003. A novel coronavirus associated with severe acute respiratory syndrome. N. Engl. J. Med. **348:**1953–1966.
44. **Lai, M. M., and S. A. Stohlman.** 1981. Comparative analysis of RNA genomes of mouse hepatitis viruses. J. Virol. **38:**661–670.
45. **Lampio, A., T. Ahola, E. Darzynkiewicz, J. Stepinski, M. Jankowska-Anyszka, and L. Kaariainen.** 1999. Guanosine nucleotide analogs as inhibitors of alphavirus mRNA capping enzyme. Antiviral Res. **42:**35–46.
46. **Langberg, S. R., and B. Moss.** 1981. Post-transcriptional modifications of mRNA. Purification and characterization of cap I and cap II RNA (nucleoside-2′-)-methyltransferases from HeLa cells. J. Biol. Chem. **256:**10054–10060.
47. **Li, J., J. S. Chorba, and S. P. Whelan.** 2007. Vesicular stomatitis viruses resistant to the methylase inhibitor sinefungin upregulate RNA synthesis and reveal mutations that affect mRNA cap methylation. J. Virol. **81:**4104–4115.
48. **Lockless, S. W., H. T. Cheng, A. E. Hodel, F. A. Quiocho, and P. D. Gershon.** 1998. Recognition of capped RNA substrates by VP39, the vaccinia virus-encoded mRNA cap-specific 2′-O-methyltransferase. Biochemistry **37:**8564–8574.
49. **Lu, Y., X. Lu, and M. R. Denison.** 1995. Identification and characterization of a serine-like proteinase of the murine coronavirus MHV-A59. J. Virol. **69:**3554–3559.
50. **Luongo, C. L., C. M. Contreras, D. L. Farsetta, and M. L. Nibert.** 1998. Binding site for S-adenosyl-L-methionine in a central region of mammalian reovirus lambda2 protein. Evidence for activities in mRNA cap methylation. J. Biol. Chem. **273:**23773–23780.
51. **Luzhkov, V. B., B. Selisko, A. Nordqvist, F. Peyrane, E. Decroly, K. Alvarez, A. Karlen, B. Canard, and J. Qvist.** 2007. Virtual screening and bioassay study of novel inhibitors for dengue virus mRNA cap (nucleoside-2′O)-methyltransferase. Bioorg Med. Chem. **15:**7795–7802.
52. **Martin, J. L., and F. M. McMillan.** 2002. SAM (dependent) I AM: the S-adenosylmethionine-dependent methyltransferase fold. Curr. Opin. Struct. Biol. **12:**783–793.
53. **Masters, P. S.** 2006. The molecular biology of coronaviruses. Adv. Virus Res. **66:**193–292.
54. **Minskaia, E., T. Hertzig, A. E. Gorbalenya, V. Campanacci, C. Cambillau, B. Canard, and J. Ziebuhr.** 2006. Discovery of an RNA virus 3′->5′ exoribonuclease that is critically involved in coronavirus RNA synthesis. Proc. Natl. Acad. Sci. USA **103:**5108–5113.
55. **Ogino, T., and A. K. Banerjee.** 2007. Unconventional mechanism of mRNA capping by the RNA-dependent RNA polymerase of vesicular stomatitis virus. Mol. Cell **25:**85–97.
56. **Pasternak, A. O., W. J. Spaan, and E. J. Snijder.** 2006. Nidovirus transcription: how to make sense? J. Gen. Virol. **87:**1403–1421.
57. **Peiris, J. S., C. M. Chu, V. C. Cheng, K. S. Chan, I. F. Hung, L. L. Poon, K. I. Law, B. S. Tang, T. Y. Hon, C. S. Chan, K. H. Chan, J. S. Ng, B. J. Zheng, W. L. Ng, R. W. Lai, Y. Guan, and K. Y. Yuen.** 2003. Clinical progression and viral load in a community outbreak of coronavirus-associated SARS pneumonia: a prospective study. Lancet **361:**1767–1772.
58. **Peyrane, F., B. Selisko, E. Decroly, J. J. Vasseur, D. Benarroch, B. Canard, and K. Alvarez.** 2007. High-yield production of short GpppA- and 7MeGpppA-capped RNAs and HPLC-monitoring of methyltransfer reactions at the guanine-N7 and adenosine-2′O positions. Nucleic Acids Res. **35:**e26.
59. **Pugh, C. S., and R. T. Borchardt.** 1982. Effects of S-adenosylhomocysteine analogues on vaccinia viral messenger ribonucleic acid synthesis and methylation. Biochemistry **21:**1535–1541.
60. **Pugh, C. S., R. T. Borchardt, and H. O. Stone.** 1977. Inhibition of Newcastle disease virion messenger RNA (guanine-7-)-methyltransferase by analogues of S-adenosylhomocysteine. Biochemistry **16:**3928–3932.
61. **Pugh, C. S., R. T. Borchardt, and H. O. Stone.** 1978. Sinefungin, a potent inhibitor of virion mRNA(guanine-7-)-methyltransferase, mRNA(nucleoside-2′-)-methyltransferase, and viral multiplication. J. Biol. Chem. **253:**4075–4077.
62. **Putics, A., W. Filipowicz, J. Hall, A. E. Gorbalenya, and J. Ziebuhr.** 2005. ADP-ribose-1″-monophosphatase: a conserved coronavirus enzyme that is dispensable for viral replication in tissue culture. J. Virol. **79:**12721–12731.
63. **Pyrc, K., B. Berkhout, and L. van der Hoek.** 2007. The novel human coronaviruses NL63 and HKU1. J. Virol. **81:**3051–3057.
64. **Quiocho, F. A., G. Hu, and P. D. Gershon.** 2000. Structural basis of mRNA cap recognition by proteins. Curr. Opin. Struct. Biol. **10:**78–86.

65. **Ramadevi, N., N. J. Burroughs, P. P. Mertens, I. M. Jones, and P. Roy.** 1998. Capping and methylation of mRNA by purified recombinant VP4 protein of bluetongue virus. Proc. Natl. Acad. Sci. USA **95:**13537–13542.
66. **Ray, D., A. Shah, M. Tilgner, Y. Guo, Y. Zhao, H. Dong, T. S. Deas, Y. Zhou, H. Li, and P. Y. Shi.** 2006. West Nile virus 5′-cap structure is formed by sequential guanine N-7 and ribose 2′-O methylations by nonstructural protein 5. J. Virol. **80:**8362–8370.
67. **Reinisch, K. M., M. L. Nibert, and S. C. Harrison.** 2000. Structure of the reovirus core at 3.6 A resolution. Nature **404:**960–967.
68. **Roussel, A., and C. Cambillau.** 1991. The TURBO-FRODO graphics package, vol. 81. Silicon graphics Geometry Partners Directory, Mountain View, CA.
69. **Sawicki, S. G., D. L. Sawicki, and S. G. Siddell.** 2007. A contemporary view of coronavirus transcription. J. Virol. **81:**20–29.
70. **Sawicki, S. G., D. L. Sawicki, D. Younker, Y. Meyer, V. Thiel, H. Stokes, and S. G. Siddell.** 2005. Functional and genetic analysis of coronavirus replicase-transcriptase proteins. PLoS Pathog. **1:**e39.
71. **Schnierle, B. S., P. D. Gershon, and B. Moss.** 1992. Cap-specific mRNA (nucleoside-O2′-)-methyltransferase and poly(A) polymerase stimulatory activities of vaccinia virus are mediated by a single protein. Proc. Natl. Acad. Sci. USA **89:**2897–2901.
72. **Schnierle, B. S., P. D. Gershon, and B. Moss.** 1994. Mutational analysis of a multifunctional protein, with mRNA 5′ cap-specific (nucleoside-2′-O-)-methyltransferase and 3′-adenylyltransferase stimulatory activities, encoded by vaccinia virus. J. Biol. Chem. **269:**20700–20706.
73. **Seybert, A., A. Hegyi, S. G. Siddell, and J. Ziebuhr.** 2000. The human coronavirus 229E superfamily 1 helicase has RNA and DNA duplex-unwinding activities with 5′-to-3′ polarity. RNA **6:**1056–1068.
74. **Shuman, S.** 1990. Catalytic activity of vaccinia mRNA capping enzyme subunits coexpressed in Escherichia coli. J. Biol. Chem. **265:**11960–11966.
75. **Shuman, S.** 2001. Structure, mechanism, and evolution of the mRNA capping apparatus. Prog. Nucleic Acid Res. Mol. Biol. **66:**1–40.
76. **Snijder, E. J., P. J. Bredenbeek, J. C. Dobbe, V. Thiel, J. Ziebuhr, L. L. Poon, Y. Guan, M. Rozanov, W. J. Spaan, and A. E. Gorbalenya.** 2003. Unique and conserved features of genome and proteome of SARS-coronavirus, an early split-off from the coronavirus group 2 lineage. J. Mol. Biol. **331:**991–1004.
77. **Söding, J., A. Biegert, and A. N. Lupas.** 2005. The HHpred interactive server for protein homology detection and structure prediction. Nucleic Acids Res. **33:**W244–W248.
78. **Thiel, V., J. Herold, B. Schelle, and S. G. Siddell.** 2001. Viral replicase gene products suffice for coronavirus discontinuous transcription. J. Virol. **75:**6676–6681.
79. **Thiel, V., K. A. Ivanov, A. Putics, T. Hertzig, B. Schelle, S. Bayer, B. Weissbrich, E. J. Snijder, H. Rabenau, H. W. Doerr, A. E. Gorbalenya, and J. Ziebuhr.** 2003. Mechanisms and enzymes involved in SARS coronavirus genome expression. J. Gen. Virol. **84:**2305–2315.
80. **van Vliet, A. L., S. L. Smits, P. J. Rottier, and R. J. de Groot.** 2002. Discontinuous and non-discontinuous subgenomic RNA transcription in a nidovirus. EMBO J. **21:**6571–6580.
81. **Vennema, H., A. Poland, J. Foley, and N. C. Pedersen.** 1998. Feline infectious peritonitis viruses arise by mutation from endemic feline enteric coronaviruses. Virology **243:**150–157.
82. **von Grotthuss, M., L. S. Wyrwicz, and L. Rychlewski.** 2003. mRNA cap-1 methyltransferase in the SARS genome. Cell **113:**701–702.
83. **Wang, H., D. Boisvert, K. K. Kim, R. Kim, and S. H. Kim.** 2000. Crystal structure of a fibrillarin homologue from Methanococcus jannaschii, a hyperthermophile, at 1.6 A resolution. EMBO J. **19:**317–323.
84. **Wang, S. P., L. Deng, C. K. Ho, and S. Shuman.** 1997. Phylogeny of mRNA capping enzymes. Proc. Natl. Acad. Sci. USA **94:**9573–9578.
85. **Woyciniuk, P., M. Linder, and C. Scholtissek.** 1995. The methyltransferase inhibitor neplanocin A interferes with influenza virus replication by a mechanism different from that of 3-deazaadenosine. Virus Res. **35:**91–99.
86. **Zhou, Y., D. Ray, Y. Zhao, H. Dong, S. Ren, Z. Li, Y. Guo, K. A. Bernard, P. Y. Shi, and H. Li.** 2007. Structure and function of flavivirus NS5 methyltransferase. J. Virol. **81:**3891–3903.
87. **Ziebuhr, J., E. J. Snijder, and A. E. Gorbalenya.** 2000. Virus-encoded proteinases and proteolytic processing in the Nidovirales. J. Gen. Virol. **81:**853–879.